Supplemental information (SI)

Obstacle-Guided Suppression of Mullins-Sekerka Instability for Freezing Purification

Hangyu Chen[1], Liang Lei[2] and Moran Wang[1]*

1Department of Engineering Mechanics and ASP, Tsinghua University, Beijing, 100084, China

2 School of Engineering, Westlake University, Hangzhou, Zhejiang, 310030, China

*E-mail: mrwang@tsinghua.edu.cn

Table of Contents

Supplementary Figures

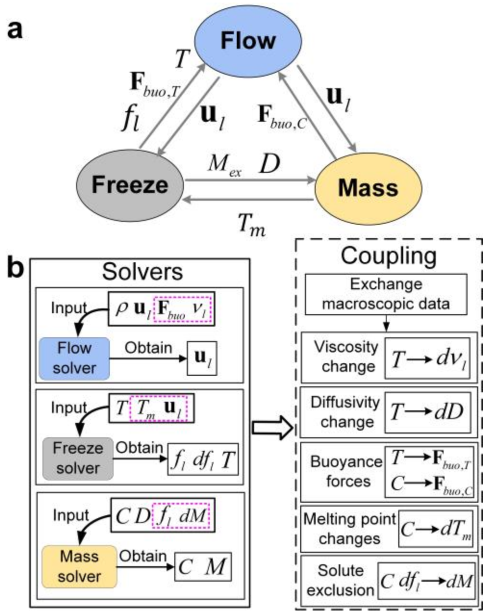

Supplementary Fig.S1 | Schematic of the novel coupled lattice Boltzmann method. **a,** Schematic of coupling among the flow, freeze, and mass solvers. T denotes temperature, F_{buo} denotes buoyancy, f_l denotes fluid fraction, u_l denotes fluid velocity, M_{ex} denotes mass exclusion, D denotes diffusivity, and T_m denotes melting temperature. **b,** Input dependencies and coupling logic. The variables highlighted in the purple dashed box require coupling operations to determine the changes in viscosity, diffusivity, buoyancy, melting temperature, and solute exclusion mass.

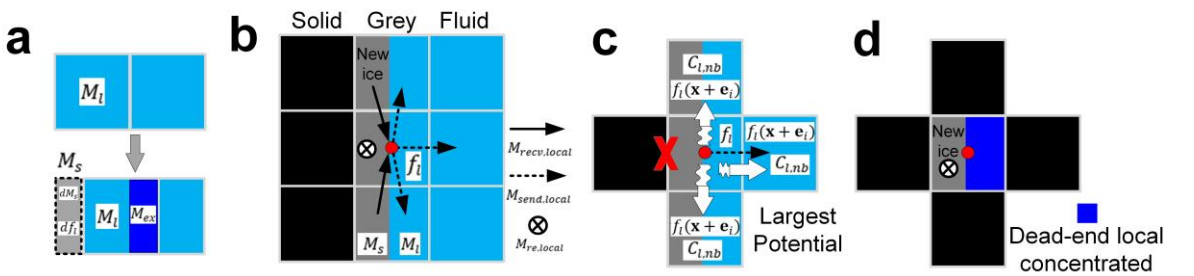

Supplementary Fig.S2 | Schematic of the novel solute exclusion method. **a,** Mass excluded to neighboring fluid node. **b,** Mass transport during freezing, expressed as the sum of mass sent to and received from neighboring nodes. **c,** Schematic of the exclusion potential applied to neighboring nodes. **d,** Mass transport for a dead-end node.

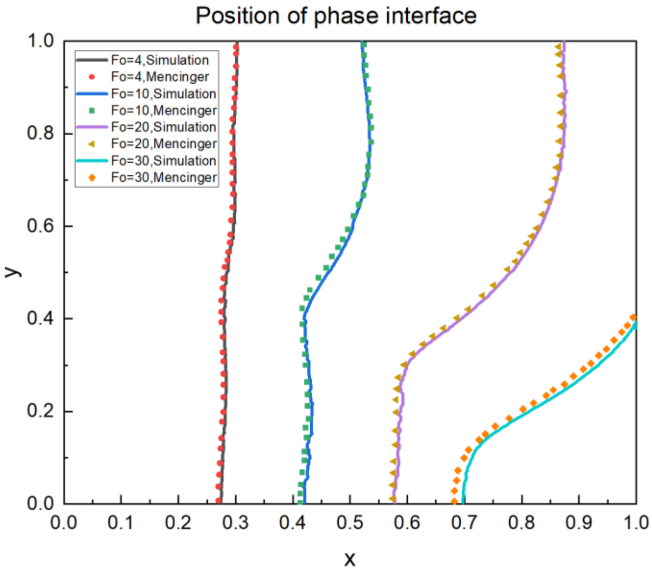

Supplementary Fig.S3 | 2D verification with Mencinger's simulation results on melting profiles. Lines are results from this simulation and the dots are Mencinger's simulation data[1].

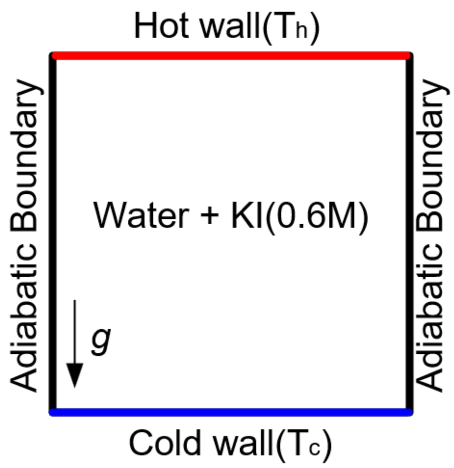

Supplementary Fig.S4 | Schematic of verification simulation setups.

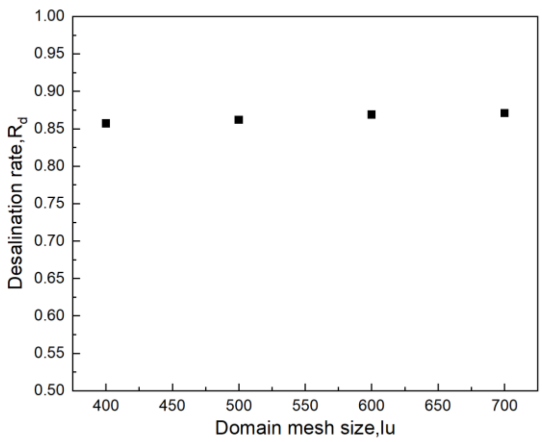

Supplementary Fig.S5 | Grid independent verification using freezing desalination with single spherical obstacle in domain mesh size from 400 lu to 700 lu.

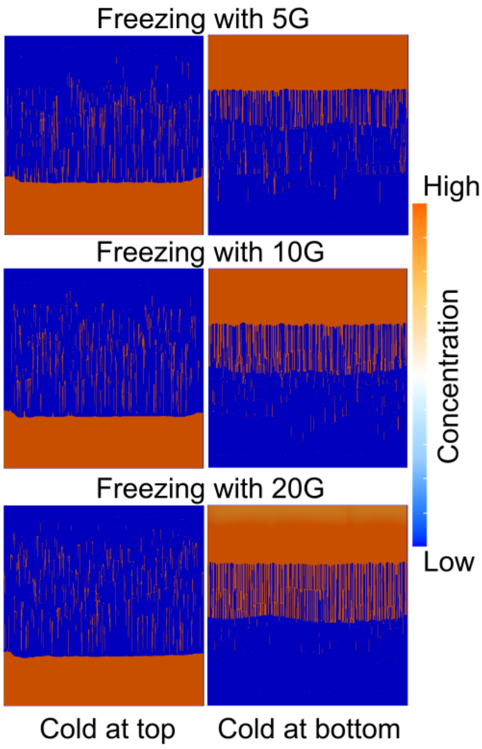

Supplementary Fig.S6 | Freeze desalination results under different gravities. Steady-state concentration distributions and brine pocket entrapment for the obstacle-free freezing desalination process with the cold source at the top (left) and at the bottom (right), under different gravitational accelerations (5G, 10G, 20G).

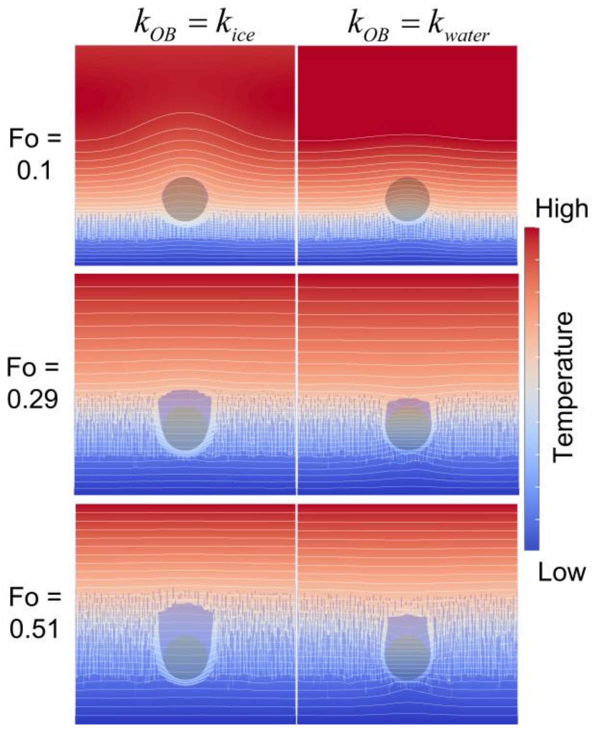

Supplementary Fig.S7 | Isotherm of the single cylinder obstacle freezing desalination at Fo = 0.1, 0.29 and 0.51.

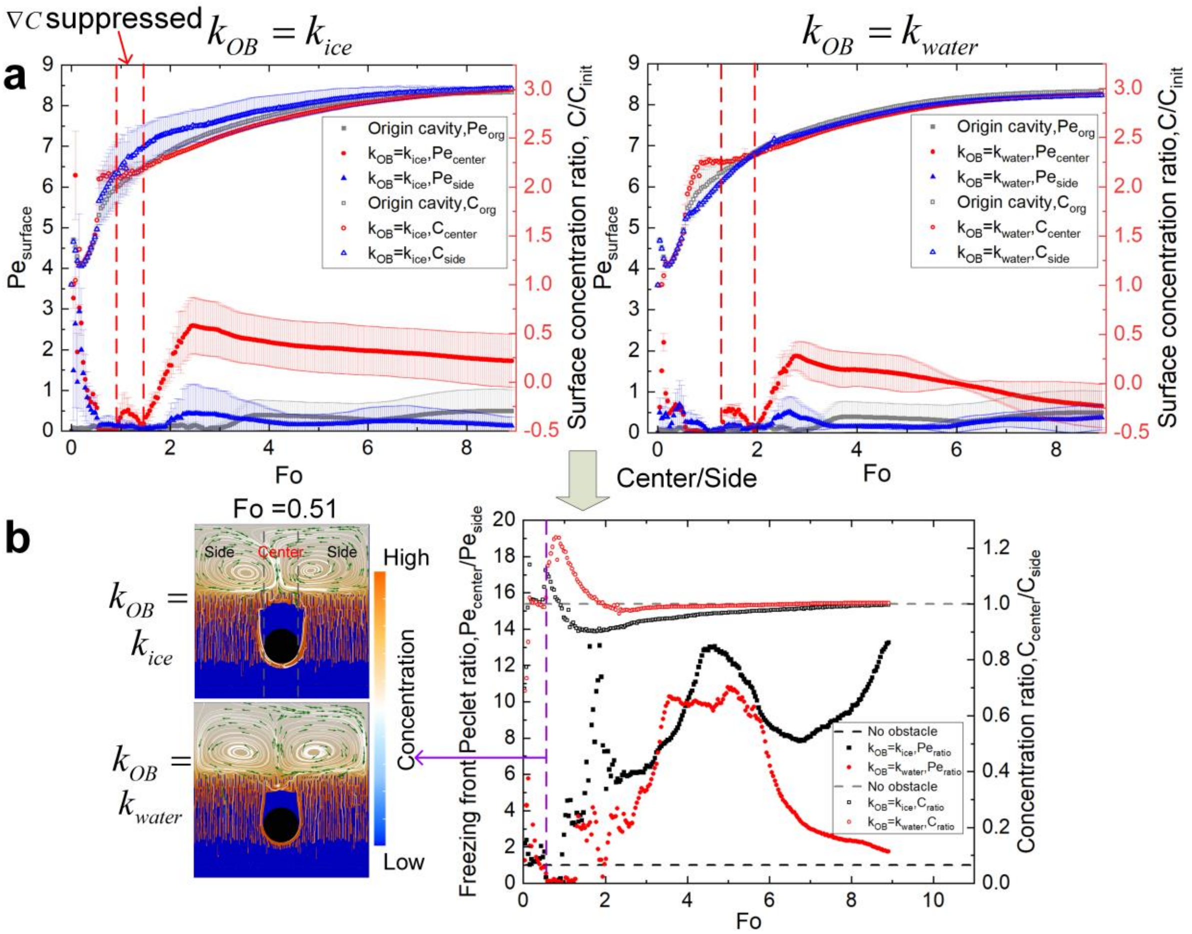

Supplementary Fig.S8 | Surface Peclet number and concentration evolution for a single cylindrical obstacle. **a,** Temporal evolutions of the surface Peclet number ($Pe_{surface}$) and normalized surface concentration (C/C_{init}) as functions of dimensionless time (Fo) at the center (behind the obstacle) and side regions (where dendrites grow), for two different obstacle thermal conductivities ($k_{OB} = k_{ice}$ and $k_{OB} = k_{water}$). **b,** Obstacle-induced relative variations in concentration and Peclet number, quantified by the ratios of center-to-side values (C_{center}/C_{side} and Pe_{center}/Pe_{side}). The inset concentration field at $Fo = 0.51$(marked by the vertical dashed purple line in the right plot) visualize the velocity patterns. Both Pe_{center}/Pe_{side} and C_{center}/C_{side} reach a minimum at this moment, followed by a sharp rise in the concentration ratio due to the suppression of convective transport.

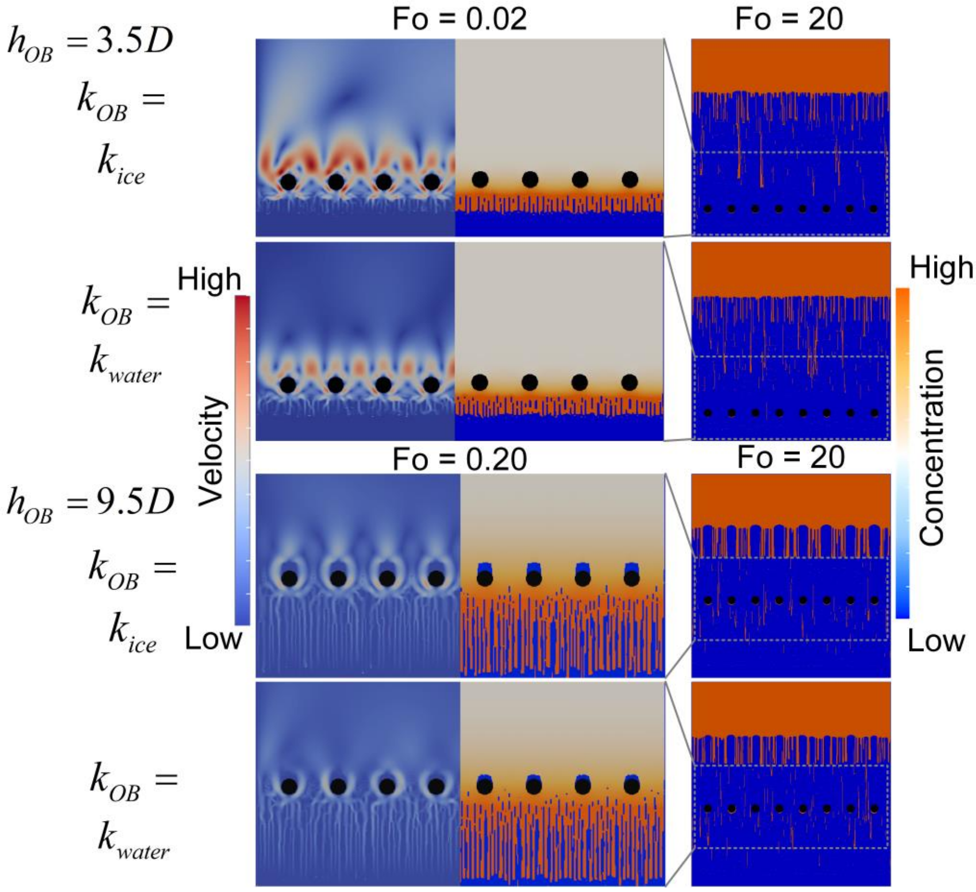

Supplementary Fig.S9 | Profiles and velocity change with different height with enlarged zone near the single-layer obstacles at Fo = 0.02 and the stable state at Fo = 20 on different height of obstacles.

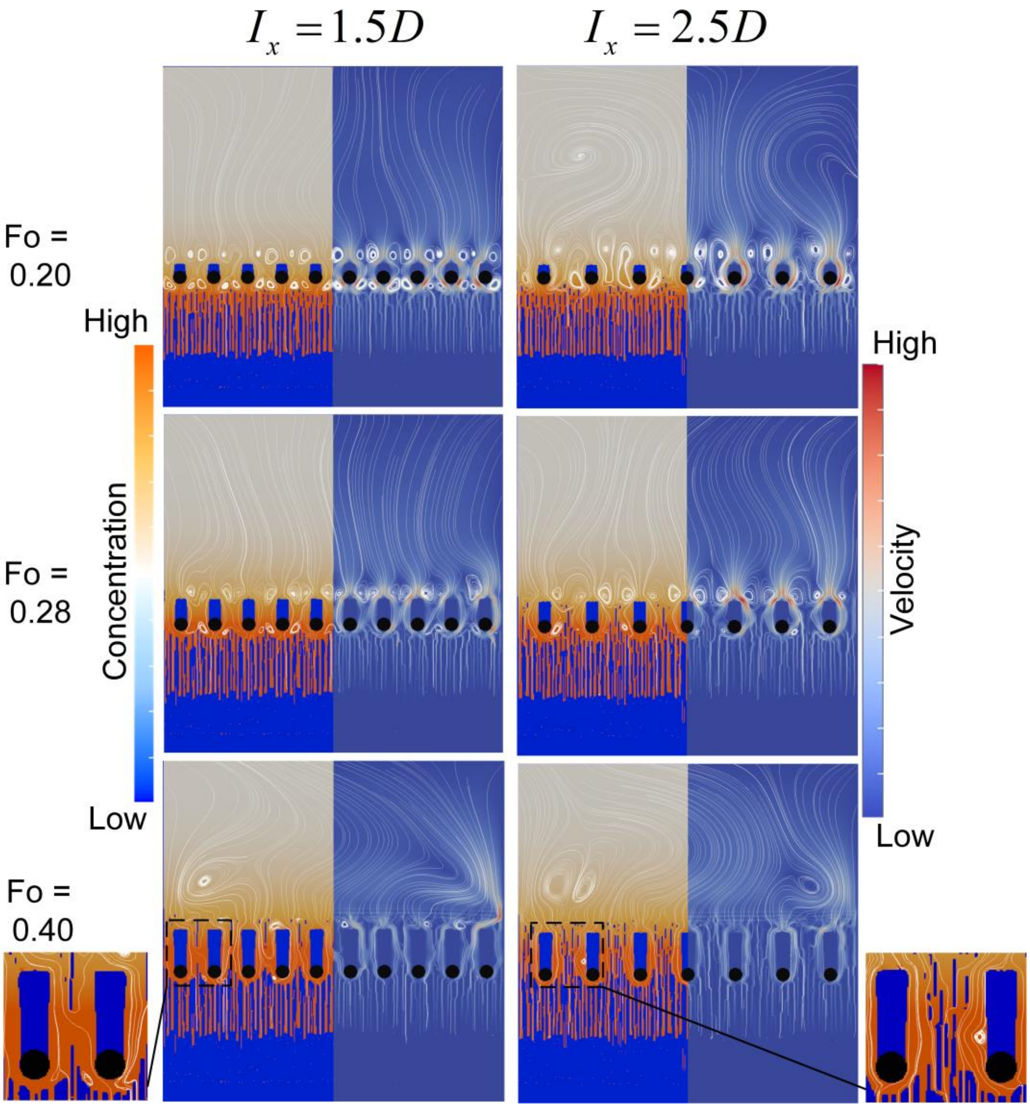

Supplementary Fig.S10 | Freezing profiles and velocity for the same height but different intervals. Stronger convection around the obstacle promotes dendritic ice growth, enhances the tendency for lateral growth, and leads to fragmented solute rejection channels between obstacles.

Supplementary Discussions

1. Definition of dimensionless numbers

The definition of the important dimensionless number Stefan number (Ste), Prandtl number (Pr), Peclet number (Pe), Fourier number (Fo), Schmidt number (Sc), Lewis number (Le), Rayleigh number of thermal convection (Ra_T) and solutal convection (Ra_s), desalination rate (R), water recovery rate (W) are defined as follow:

$$Ste = \frac{c_{p,l}(T_h - T_c)}{La}, \tag{S1}$$

$$Pr = \frac{\nu_l}{\alpha_l}, \tag{S2}$$

$$Pe = \frac{u_l}{D_c}, \tag{S3}$$

$$Fo = \frac{\alpha_l t}{l_d^2}, \tag{S4}$$

$$Sc = \frac{\nu_l}{D_c}, \tag{S5}$$

$$Le = \frac{Sc}{Pr} = \frac{\alpha_l}{D_c}, \tag{S6}$$

$$Ra_T = \frac{(T_h - T_c)\beta_{water} l_d^3 |\mathbf{g}|}{\nu_l \alpha_l}, \tag{S7}$$

$$Ra_s = \frac{|\mathbf{g}| \beta_c \Delta C l_d^3}{\nu_l D_c}. \tag{S8}$$

Here, the $c_{p,l}$ is the specific heat of liquid, T_h is the hot source temperature, T_c is the cold source temperature, La is the latent heat, ν_l is the viscosity of the liquid, α_l is the thermal diffusivity of the liquid, D_c is the constant diffusivity of solute, l_d is the characteristic length of the domain, β_{water} is the coefficient of thermal expansion, β_c is the solutal expansion coefficient, t is the time, $\mathbf{g}$ is the gravity, ΔC is the concentration difference.

The desalination rate R, is defined as

$$R = (1 - \frac{M_{ice}}{M_0}). \tag{S9}$$

Here, M_0 is the initial total solute mass and M_{ice} is the mass of the solute trapped in the ice.

The water recovery rate W, is defined as

$$W = \frac{V_{ice}}{V_0}. \tag{S10}$$

Here, the V_{ice} is the ice-covered volume which includes the brine pockets trapped by ice, V_0 is the initial volume.

2. Numerical methods

The coupling model is described as Fig.S1. The lattice Boltzmann method (LBM) is well suited for multiphase phase-change problems because of its natural coupling of flow, heat transfer, and interface evolution[2,3]. This simulation consists three coupled solvers which are flow, freeze and mass to control the fluid flow, freezing process and solute transport respectively. In this study, the simulation domains are layers of 3D cases with periodic boundary at z direction. The discrete D3Q19[4] is used in flow and freeze solver. The D3Q7 is used in mass solver. The basic models are same as a former article of the author[5].

After the basic LBEs of the solvers, the coupling between solvers is also significant and decides the correct solute transport during phase change[6]. The coupling between solvers should be executed after the whole computation step of all solvers.

To couple the fluid fraction change and realize the nonslip velocity condition in the solid phase, the density distribution of flow is recalculate after streaming[7], the final density distribution function f_i is recalculated by the following linear interpolation based on the liquid fraction

$$f_{i,sf} = f_l f_i^* + (1 - f_l) f_i^{eq}(\rho, \boldsymbol{u}_s). \tag{S11}$$

Here, $f_{i,sf}$ is the modified distribution function, f_i^* is the post-streaming distribution function, $\boldsymbol{u}_s$ is the solid velocity.

It should be noticed that the coupling of fluid fraction and the boundary condition on the liquid-solid interface can also be realized by the immersed moving boundary (IMB) [8,9], a lattice node can be a pure fluid, a pure solid or a mixed node. In normal melting cases, IMB only shows very small difference with the one with recalculation after streaming. To ensure the consistency of the coupling structure and appropriately reduce the computational cost, IMB is adopted. It modified the collision operator and source term with the solid fraction and the LBE becomes (single-phase as example):

$$f_i(\boldsymbol{x} + \boldsymbol{e}_i \delta_t, t + \delta_t) = f_i(\boldsymbol{x}, t) + \left(1 - B_f\right)\Omega_i^f + B_f \Omega_i^{fs} + \left(1 - B_f\right)\delta_t \tilde{F}_i, \tag{S12}$$

The collision operator Ω_i^f (fluid) is defined as

$$\Omega_i^f = -\frac{1}{\tau_f}\left[f_i(\boldsymbol{x}, t) - f_i^{eq}(\boldsymbol{x}, t)\right], \tag{S13}$$

The collision operator Ω_i^{fs} for solid nodes is defined as

$$\Omega_i^{fs} = f_{-i}(\boldsymbol{x}, t) - f_i(\boldsymbol{x}, t) + f_i^{eq}(\rho, \boldsymbol{u}_b) - f_{-i}^{eq}(\rho, \boldsymbol{u}), \tag{S14}$$

$$B_f = \frac{\varepsilon_s(\tau_f - 0.5)}{(1 - \varepsilon_s) + (\tau_f - 0.5)}, \tag{S15}$$

To describe the exclusion effect of ice growth, IMB [8,9] is also used to provide an interface for the transport of solute as the volume fraction of the ice changes. The LBE of the mass solver also changes as

$$g_i(\mathbf{x}+\mathbf{e}_i\delta_t, t+\delta_t) = g_i(\mathbf{x}, t) + (1-B_g)\Omega_i^g + B_g\Omega_i^{gs} + \delta_t\tilde{S}_i, \tag{S16}$$

$$\Omega_i^g = -\frac{1}{\tau_g}\left[g_i(\mathbf{x}, t) - g_i^{eq}(\mathbf{x}, t)\right], \tag{S17}$$

$$\Omega_i^{gs} = g_{-i}(\boldsymbol{x}, t) - g_i(\boldsymbol{x}, t) + g_i^{eq}(C, \boldsymbol{u}_b) - g_{-i}^{eq}(C, \boldsymbol{u}), \tag{S18}$$

$$B_g = \frac{\varepsilon_s(\tau_g - 0.5)}{(1-\varepsilon_s)+(\tau_g-0.5)}. \tag{S19}$$

Here, the extra source term $\tilde{S}_i = \omega_i q$, q is the mass change each time, ε_s is the solid fraction, $\boldsymbol{u}_b$ is the solid boundary velocity. The concentration of the local node C is still $C = \sum_i g_i$, but the mass of the solute is separated to two parts: mass in fluid (M_l) and mass in solid (M_s). If the volume of the local node is 1 then $C = M_l + M_s$. In order to achieve the solute exclusion by the ice generation, we assume the exclusion follows principles:

1) The generation of the ice push part of the solute out of freezing nodes to the surrounding fluid nodes, the ratio of the solute remains stationary is defined as residue coefficient k_r and the excluded ratio is $(1 - k_r)$.

2) The residue solute exists in the ice and release when it melts to fluid node. The mass of residue trapped each time in the freezing process link with the local concentration of each node.

3) The exclusion process ensures the mass conservation and no solute pass through the pure solid interface.

To ensure the solid-liquid interface becomes an impenetrable boundary for the solute, an extra boundary treatment on the pure solid wall and grey nodes is applied as

$$f_{s,-i}(\mathbf{x}+\mathbf{e}_i, t) = f_{l,i}(\mathbf{x}, t), \tag{S20}$$

$$f_{l,-i}(\mathbf{x}, t+dt) = f_{s,-i}(\mathbf{x}+\mathbf{e}_i, t). \tag{S21}$$

Which can be a simple bounce-back version or more complex in other cases if consider the penetration at the boundary.

It should be noticed that the residue coefficient k_r show similar but different physical meaning as the effective partition(distribution) coefficient K_{eff} which is defined as the ratio of the ice salinity C_{ice} to the salinity of the remaining concentration solution C_l. K_{eff} should be very small at the pure ice-water sharp interface. However, in this model, the residue coefficient k_r means the solute trapped at the local node with the ice-water interface which can includes small brine pockets that cannot be distinguished under this resolution.

During the freezing process, the solute is gradually excluded from the local node and pushed to the neighbor liquid node. The mass excluded by the freezing is described as Fig.S2(a) and calculated as

$$M_{send} = M_{ex} = -(1-k_r)\frac{df_l}{f_l - df_l}(C - M_s). \tag{S22}$$

The mass residue with freezing is calculated as

$$M_{re,local} = -k_r\frac{df_l}{f_l - df_l}(C - M_s), \tag{S23}$$

for a node, the mass received from all neighbors is

$$M_{recv} = \sum_{nb} M_{ex\rightarrow local}, \tag{S24}$$

Finally, the value q of local node is as sum of solute send and receive as shown in Fig.S2(b) and is expressed as

$$q = M_{send} + M_{recv}. \tag{S25}$$

The direction of mass exclusion is decided by both free space and concentration of neighbor nodes. The local liquid part concentration $C_l = M_l/f_l$, which decided the concentration contribution from the fluid phase. To decide the exclusion direction of solute, an exclusion potential $P_{ex,i}$ which represent the potential to exclude to i direction is proposed as

$$P_{ex,i} = \alpha f_l(\mathbf{x} + \mathbf{e}_i) + \beta C_l(\mathbf{x} + \mathbf{e}_i). \tag{S26}$$

Where $\alpha = 1.0$, $\beta = -0.01$. The $P_{ex,i}$ means the exclusion direction mainly decided by the empty space of neighbors but also influenced by concentrations with different contributions. Here, fore pure solid node or fixed wall, the $P_{ex,i} = -\infty$. The excluded solute shall be pushed to the largest potential neighbor node as shown in Fig.S2(c). If a node is surrounded by pure solids or fixed wall nodes, the node is a dead end and shall pass no solute to its neighbors, all excluded mass shall be stored locally as shown in Fig.S2(d).

3. Model verifications and setups

Our LBM model was validated against the classical simulation of tin melting by Mencinger et al[1] as shown in Fig.S3. The results, presented on the left figure, demonstrate that our simulation results (lines) for the melting front evolution and rate closely match the established control volume method results (dots) at Ra = 25000, Pr = 0.02 and Ste = 0.01.

Supplementary Table. S1 | Simulation setups and dimensionless number comparison of the verification with experiment data [10].

Key parameters	Experiment	Simulation
Size	1 cm (0.01m)	400 lu
dT	[-9,0] °C, $T_l = 4$°C	[0,1], $T_l = 1.4477$
Concentration	0.6 mol/L	1.0
ν	$1.787 \times 10^{-6} m^2/s$	1.5
α	$1.32 \times 10^{-7} m^2/s$	0.111
D	$1.0 \times 10^{-9} m^2/s$	0.01
Ste	0.1125	0.1125
Ra_T	18695.6	18695.6
Ra_s	368528259.7	373912.6
Pr	13.5	13.5
Sc	1787	150
Le	132	11.08

Due to the simulation cost and stability the, the $Ra_s = 20Ra_T$, and Sc, Le are all smaller than reality. $k_r = 0.02$. The simulation setups are described as Fig.S4.

4. Grid independent verification

To ensure grid-independent results, we verified desalination rate for a single spherical obstacle case with diameter $D = 0.2l_d$ varied by less than 2% across grid resolutions from 400 to 700 *lu* as shown in Fig.S5. Based on this, a resolution of 500 *lu* is adopted for origin simulations to ensure accuracy while maintaining computational efficiency.

5. Different gravity effects

Freeze concentration results under varying gravity levels indicate that stronger convection universally enhances dendritic growth as Fig.S6. When the cold source is at the top, increased convection obviously shortens the transition layer, intensifies the brine pocket layer, and aggravates brine entrapment. In contrast, with the cold source at the bottom, stronger convection expands the initially pure ice zone but promotes more pronounced dendritic growth near the top of the ice layer.

6. Zero-dimensional model

A zero-dimensional (0D) model based on the heat flux balance and the semi-infinite plate assumption is proposed to predict the edge line of the pure ice zone behind the spherical obstacle. There are several assumptions:

1) The freezing point temperature is the corresponding T_m with the modification of concentration.

2) The obstacle close to the cold source and the freezing system around it is a semi-infinite flat freezing.

3) The freezing node is affected by three heat flux: inner obstacle projection zone q_{in}, outer heat flux q_{out}, cold-heat heat flux q_y. The ice generation direction is decided by the vector sum of heat fluxes.

4) There is a damping on x direction to decrease the total heat flux on $q_{x,total}$, the end distance is about 0.73 to 1.27(based on simulation). Ice growth is decided by the heat flux.

5) The start point of icing on obstacle is start on the edge of cylinder.

The clean ice edge starts from the B point but the vector of the heat flux is unknown, assume the outer ice reaches the same height, the concentration at the interface is higher than the bulk and it assume to be the same concentration C_{max}, then the melting point $T_{m,B}$ at B can be calculated.

$$C_B = C_{max} = 2C_0, T_{m,B} = T_{m,org} + C_B K_c. \tag{S27}$$

Here, C_0 is the initial concentration and K_c is the decreasing of melting point with concentration, $T_{m,org}$ is the origin melting point without solute. The semi-infinite freezing height $s(t)$ follows[11]

$$s(t) = 2\lambda\sqrt{\alpha_s t}. \tag{S28}$$

For small Ste number, use approximate number $\lambda = \sqrt{Ste/2}$, then the time $t = L_{start}/2Ste\alpha_s$ is the start time t_{start}, H_o is distance of the center point O with cold source. Then, use semi-infinite to compute the outer temperature T_{out} with time[11]

$$T_{out} = T_{cold} + \left(T_{org} - T_{cold}\right)\mathrm{erf}\left(\frac{H_o}{2\sqrt{\alpha_{eff,out} t_{start}}}\right). \tag{S29}$$

Here, the $\alpha_{eff,out} = \alpha_{ice}$, T_{cold} is the cold source. The heat flux q_{out} are calculated with Fourier's law

$$q_{out} = k_{out}\frac{T_{out}-T_{m,B}}{L_{out}}. \tag{S30}$$

Here, $L_{out} = (0.5D_m - R)/2$, R is the radius of cylinder, D_m is the domain size, D_s is the diameter of sphere, $k_{out} = k_{ice}$. Then the inner heat flux q_{in} is calculated as

$$q_{in} = k_{in}\frac{T_O-T_{m,B}}{L_{in}}. \tag{S31}$$

The temperature of the center T_O is

$$T_o = T_{cold} + \left(T_{org} - T_{cold}\right)\mathrm{erf}\left(\frac{H_P+D_s/2}{2\sqrt{\alpha_{eff,in}t}}\right). \tag{S32}$$

Here, the effective thermal conductivity of inner $\alpha_{eff,in} = (H_P\alpha_{ice} + D_s\alpha_{OB})/(H_P + D_s)$, $L_{in} = 0.5D_s$ and $k_{in} = k_{fix}$, H_P is the distance of the bottom point P with cold source, α_{OB} is the thermal diffusivity of the obstacle. The main heat flux on y direction q_y is

$$q_y = k_{ice}\frac{T_{cold}-T_{m,B}}{H_O}. \tag{S33}$$

Here, $L_y = H_O$ and $k_y = k_{ice}$.

The component at the x and y directions are

$$q_{y,total} = q_y, \tag{S34}$$

$$q_{x,total} = q_{in} - q_{out}. \tag{S35}$$

However, there is an empirical coefficient to modify the heat flux at x direction due to semi-infinite assumption $q_{x,init} = 0.4q_{x,total}$. The ice generation is assumed to be decided by the heat flux and decide the next ice edge position.

After the start point B, the next clean ice edge point influenced by the former heat flux. In the simulation, no matter positive or negative of heat flux at x direction, there is always a damping to 0. There is an assumption that when the out and projection zone ice height are close (influence of the obstacle is weak), then the x direction has not heat flux. Then, the distance between out and in can be used to calculated the equilibrium time t_{eq}, the growth of the ice is calculated by the semi-infinite assumption.

$$s_{out}(t) = 2\lambda\sqrt{\alpha_s t_{eq}}, \tag{S36}$$

$$s_{in}(t) = D_s + 2\lambda\sqrt{\alpha_{in,eff}t_{eq}}, \tag{S37}$$

$$\alpha_{in,eff} = \frac{\alpha_{ice}(H_P)+D_s\alpha_{OB}}{D_s+H_P}, \tag{S38}$$

$$0.73 < \frac{s_{out}(t)}{s_{in}(t)} < 1.27. \tag{S39}$$

Then, with Eq. S (36) to S (39) the equilibrium time t_{eq} is obtained, the prediction time of the ice growth balance after start time $t_{eq,remain}$ can be obtained as

$$t_{eq,remains} = t_{eq} - t_{start}. \quad \text{(S40)}$$

Use an empirical coefficient (1/3) to achieve shorter time with convection effect

$$t_{eq,balance} = t_{eq,remains}/3. \quad \text{(S41)}$$

After the t_{eq}, there is no heat flux at x direction, the damping at x direction is described as

$$q_{x,total(new)} = q_{x,init}(1 - \frac{t-t_{start}}{t_{eq,balance}})^n, n = 2. \quad \text{(S42)}$$

The heat flux at y direction also influenced by the material below it. If it has effective thermal conductivity $k_{eff,y}$

$$k_{eff,y} = \frac{(I_y-L_{B,chord})k_{ice}+L_{B,chord}k_{fix}}{I_y}. \quad \text{(S43)}$$

Here, $L_{B,chord}$ is the chord length on sphere if the point B moves to the projection zone of sphere. Then, compute the coordinate I of new clean ice edge with heat flux and old position

$$I_{x,new} = I_{x,old} + d_x, \quad \text{(S44)}$$

$$I_{y,new} = I_{y,old} + d_y, \quad \text{(S45)}$$

$$d_x = \frac{q_{x,total}dt}{\rho L_a}. \quad \text{(S46)}$$

Finally, the clean ice edge (I_x, I_y) can be calculated with time increasing and draw the edge line after the initial ice point.

7. Surface Péclet of single sphere obstacle

As shown in Fig.S8, the surface Péclet number ($Pe_{surface}$) and the interfacial concentration at the center behind the obstacle (pure ice zone) and at the side (dendritic growth zone) results, it is clear that there exists a period during which the concentration gradient at the top of the center is suppressed by convection, causing the concentration profile to become more gradual over time; this occurs for both types of obstacles. The center-to-side ratios show that the obstacle induces a concentration difference between the center and the side, which eventually approaches equilibrium. The convection at the center surface is stronger and lasts longer than in the low thermal conductivity case.

When the freezing reaches instability point ($Fo = 0.51$), the dendrites emerge at the top and begin to shield the interface from the effect of convection, thereby reducing the concentration perturbation near freezing front. With the freezing process, the concentration gradient is larger which also means higher convection intensity. It can promote the lateral growth of dendrites in the area close to the final ice line. Blockage in the final salt exclusion stage tends to cause extensive trapping of high concentration brine pockets.

8. Different obstacle height effects

When the height is lower, the ice growth rate upon contact is faster and the convection intensity is stronger as shown in Fig.S9. As a result, a single-layer spherical obstacle array provides only limited optimization of the solute exclusion pathways near the bottom. When the array is positioned close to the brine pocket region, brine entrapment inevitably occurs in the inter-obstacle gaps and at the bottom.

9. Different obstacle interval effects

When the ice grows around the obstacles, stronger convection promotes dendritic ice formation and enhances the tendency for lateral growth, which can easily disrupt the solute exclusion channels as shown in Fig.S10. A larger lateral spacing between obstacles intensifies convection and leads to more fragmented channels, whereas an excessively narrow intervals blocks the upward transport of solute from the bottom through the interstices of the obstacle array. This phenomenon also explains why a staggered arrangement improves the desalination rate: the staggered structure effectively reduces the effective lateral intervals, which is blocked by the ice growing from the bottom in an alternating pattern, yet without obstructing the upward exclusion channel at the bottom. It also restricts convection while still allowing salt to be excluded. Therefore, convection in the middle and even at the bottom of the porous medium is detrimental. In contrast, convection near the top is beneficial, as it helps carry away the excluded solute, and the slow freezing rate there enhances the effective diffusion coefficient.

References

1 Mencinger, J. Numerical simulation of melting in two-dimensional cavity using adaptive grid. *Journal of Computational Physics* **198**, 243-264 (2004).

2 Huang, J., Wang, L., Chai, Z. & Shi, B. Phase-field-based lattice Boltzmann method for containerless freezing. *Physical Review E* **110**, 035301 (2024).

3 Zhao, Y., Pereira, G. G., Kuang, S., Chai, Z. & Shi, B. A generalized lattice Boltzmann model for solid–liquid phase change with variable density and thermophysical properties. *Applied Mathematics Letters* **104**, 106250 (2020).

4 d'Humières, D. Multiple–relaxation–time Lattice Boltzmann Models in Three Dimensions. *Philosophical Transactions of the Royal Society of London* **360**, 437-451 (2002).

5 Chen, H. & Wang, M. Non-monotonic ice-core thawing in water pool driven by competition between anomaly-triggered chaotic flow and normal natural convection. *Journal of Fluid Mechanics* **1031**, A51 (2026).

6 Wu, J., Sun, D., Chen, W. & Chai, Z. A unified lattice Boltzmann-phase field scheme for simulations of solutal dendrite growth in the presence of melt convection. *International Journal of Heat and Mass Transfer* **220**, 124958 (2024).

7 Huang, R. & Wu, H. Total enthalpy-based lattice Boltzmann method with adaptive mesh refinement for solid-liquid phase change. *Journal of Computational Physics* **315**, 65-83 (2016).

8 Noble, D. & Torczynski, J. A lattice-Boltzmann method for partially saturated computational cells. *International Journal of Modern Physics C* **9**, 1189-1201 (1998).

9 Xia, M. *et al.* A coupled DEM-IMB-LBM model for simulating methane hydrate exploitation involving particle dissolution. *International Journal for Numerical Methods in Engineering* **124**, 1701-1720 (2023).

10 Wu, Z. *et al.* Microscopic salt exclusion dynamics of directional freezing in brine. *Journal of Fluid Mechanics* **1021**, A15 (2025).

11 Carslow, H., Jaeger, J. C. & Morral, J. Conduction of heat in solids. *Journal of Engineering Materials and Technology* **108**, 378-378 (1986).